Model and performance evaluation of field-effect transistors based on epitaxial graphene on SiC

Martina Cheli, Paolo Michetti and Giuseppe Iannaccone
Dipartimento di Ingegneria dell'Informazione: Elettronica, Informatica, Telecomunicazioni, via Caruso 16, 56100 Pisa, Italy
email: {martina.cheli, paolo.michetti, g.iannaccone}@iet.unipi.it

arXiv:0909.4678v1 [cond-mat.mes-hall] 25 Sep 2009

Abstract

In view of the appreciable semiconducting gap of 0.26 eV observed in recent experiments, epitaxial graphene on a SiC substrate seems a promising channel material for FETs. Indeed, it is two-dimensional - and therefore does not require prohibitive lithography - and exhibits a wider gap than other alternative options, such as bilayer graphene. Here we propose a model and assess the achievable performance of a nanoscale FET based on epitaxial graphene on SiC, conducting an exploration of the design parameter space. We show that the current can be modulated by 4 orders of magnitude; for digital applications an $I_{\rm on}/I_{\rm off}$ ratio of 50 and a subthreshold slope of 145 mV/decade can be obtained with a supply voltage of 0.25 V. This represents a significant progress towards solid-state integration of graphene electronics, but not yet sufficient for digital applications.

I. Introduction

Epitaxially grown graphene on SiC provide potential for large scale integration of graphene electronics. The first challenge to the use of graphene as a channel material for FETs is to induce a reasonable gap for room temperature operation. Recently Zhou *et al.* [1] have experimentally demonstrated that a graphene layer, epitaxially grown on a SiC substrate, can exhibit a gap of about 0.26 eV, measured by angle-resolved photo-emission spectroscopy. The gap is probably due to symmetry breaking between the two sublattices forming the graphene crystalline structure, as also confirmed by recent density functional calculations [2], [3]. According to the authors of Ref. [1], this method of inducing a gap is very easy and reproducible; in addition, the thickness of graphite grown on SiC can be precisely controlled to be either single- or multiply layered depending on growth parameters [4]. From a manufacturability point of view it is also extremely promising, since it would be highly convenient to prepare an entire substrate of graphene on an insulator and then obtain single device and integrated circuit through patterning [5].

From its isolation [6], [7], graphene has attracted the attention of the scientific community due to its exceptional physical properties, such as an electron mobility exceeding more than 10 times that of silicon wafers [8], and in view of its possible applications in transistors [9] and in sensors [10]. To induce a gap in graphene structures, several methods have been used: lateral confinement in graphene ribbons [9], [11] carbon nanotubes [12], impurity doping [13], or a combination of single and bilayer graphene regions [14], [15], [16]. Unfortunately, they all face different problems.

Carbon nanotubes exhibit large intrinsic contact resistance and are difficult to pattern in a reproducible way; the inability to control tube chirality, and thus whether or not they are metallic or semiconducting, make solid state integration still prohibitive. Graphene nanoribbons [9], [11] allow to obtain a very interesting device behavior [17], but require extremely narrow ribbons with single-atom precision, since a difference of only one dimer line in the width may yield a quasi-zero gap nanoribbon. Bilayer graphene exhibits a gap in the presence of a perpendicular electric field, but the range of applicable bias can only induce a gap of $100-150$ meV, not sufficient to obtain a satisfactory behavior in terms of $I_{\rm on}/I_{\rm off}$ ratio [15]. Graphene on SiC can is a two-dimensional material, thus does not require extremely sophisticated lithography, and provides a higher energy gap: for the sake of comparison, a 0.26 eV energy gap would require an armchair nanoribbon of width smaller than 3 nm, or nanotubes with diameter smaller than 2 nm.

In this work we present a semi-analytical model of an FET with a channel of epitaxial graphene grown on a SiC substrate, where the band structure, the electrostatics, thermionic and band-to-band tunneling currents are carefully

accounted for. On the basis of our model, we assess the achievable device performance through an exploration of the device parameter space, and gain understanding of the main aspects affecting device operation.

II. MODEL

We adopt the Tight Binding (TB) Hamiltonian for single layer graphene on SiC that was proposed by Zhou *et al.* [1]. The empirical TB valence $(-)$ and conduction $(+)$ bands of a single epitaxial layer of graphene on SiC, read:

$$E_{\pm}(k_x, k_y) = \pm\sqrt{m^2 + t^2|f(\mathbf{k})|^2}, \tag{1}$$

where t is the in-plane hopping term (2.7 eV), $m = 0.13$ eV is an empirical potential energy shift between the two inequivalent graphene sublattices due to interaction with the SiC substrate, and $f(\mathbf{k})$ is the off-diagonal element of the considered Hamiltonian [1]. In the six Dirac points of the graphene Brillouin zone, where $f(\mathbf{k})$ is zero, there is a finite energy gap $E_g = 2m$, corresponding to the channel conduction minimum $E_{CC} = m - q\phi_{ch}$ and the channel valence maximum $E_{VC} = -m - q\phi_{ch}$, where q is the electron charge and ϕ_{ch} the self-consistent potential in the central region of the channel.

The device under consideration, depicted in 1(a), is a transistor with a channel of epitaxial graphene on a SiC substrate of thickness $t_{sub} = 100$ nm, with a top gate separated by a SiO_2 layer of thickness t_{ox}. In 1(b) we have sketched the band edge profiles along the transport direction $\hat{x}$, where E_{Ci} and E_{Vi} respectively represent the conduction and valence band edges in the three different regions denoted by i=S, D, C (Source, Drain, Channel). Source and drain contacts are n^+ doped, with molar fraction α_D, which translates into an energy difference A between the electrochemical potential μ_S (μ_D) and the conduction band edge E_{CS} (E_{CD}) at the source (drain) contact. The potential is set to zero at the source and to V_{ds} at the drain contact. In the center of the channel ϕ_{ch} is imposed by vertical electrostatics. We assume, as usual, complete phase randomization along the channel, which is particularly important because it allows us to neglect the effect of resonances in the presence of tunneling barriers.

Exploiting the Gauss theorem we can write the surface charge density in the central part of the channel as

$$Q = -C_g\left(V_g - V_{FBt} - \phi_{ch}\right) - C_{sub}\left(V_{sub} - V_{FBb} - \phi_{ch}\right), \tag{2}$$

where $C_g = \epsilon_{SiO_2}/t_{ox}$ ($C_{sub} = \epsilon_{SiC}/t_{sub}$) is the capacitance per unit area between the channel and the top gate (back gate), V_g (V_{sub}) is the top gate (back gate) voltage, V_{FBt} (V_{FBb}) is the flat-band voltage of the top gate (back gate), which we set to -0.4 eV.

The transit time of the device in the channel has been estimated as $\tau_t = \frac{Q_{th}L_C}{J_{th}} \approx 10^{-16}$ s where Q_{th} and J_{th} are the thermionic charge and current, respectively, $L_C = 20$ nm is the channel length.

In certain spectral regions, for example in the valence band when the device is in the off state, carriers are quasi confined by tunneling barriers, and can dwell in the channel for a much longer time and be subject to some degree of inelastic relaxation, even if transport in the conduction band is practically ballistic. To consider this effect, we have therefore included a degree of inelastic scattering that leads to energy relaxation.

In steady-state conditions, considering an infinitesimal element of area $dk_x dk_y$ in the wave-vectors space, charge distribution in the channel is obtained as a balance between two types of charge exchange processes with the contacts: one elastic, and one inelastic.

We can write the electron charge in the channel as the sum of two contributions: N^e_+ and N^e_-. $N^e_+ = f^e_+ L_C n_{2D}$ ($N^e_- = f^e_- L_C n_{2D}$) represents the density of forward (backward) going electrons, $f^e_{\pm}(k_x, k_y)$ denotes the occupation factors of forward $(+)$ and backward $(-)$ states in the channel and $n_{2D}(k_x, k_y)$ is the 2-dimensional density of states in the k-space. For each contribution we can write a rate equation in steady-state conditions:

$$\frac{dN^e_+}{dt} = J^+_S - J^+_D + (1 - T_S) f^e_- v_x - (1 - T_D) f^e_+ v_x + \frac{f^e_S - f^e_+}{\tau_S} L_C n_{2D} = 0 \tag{3}$$

$$\frac{dN^e_-}{dt} = -J^-_S + J^-_D - (1 - T_S) f^e_- v_x + (1 - T_D) f^e_+ v_x + \frac{f^e_D - f^e_-}{\tau_D} L_C n_{2D} = 0 \tag{4}$$

where: $f^e_{D,S} = \mathfrak{F}\left(E_+ - q\phi_{ch} - \mu_{D,S}\right)$ is the occupation factor at the drain (D) and source (S) contacts, and $\mathfrak{F}$ is Fermi-Dirac distribution function.

Let us focus on eq. 3 (similar considerations can be made for eq. 4): $J^+_S = T_S f^e_S v_x$ is the tunneling current component injected from source, $J^+_D = T_D f^e_+ v_x$ is instead the drain tunneling current component ejected to the

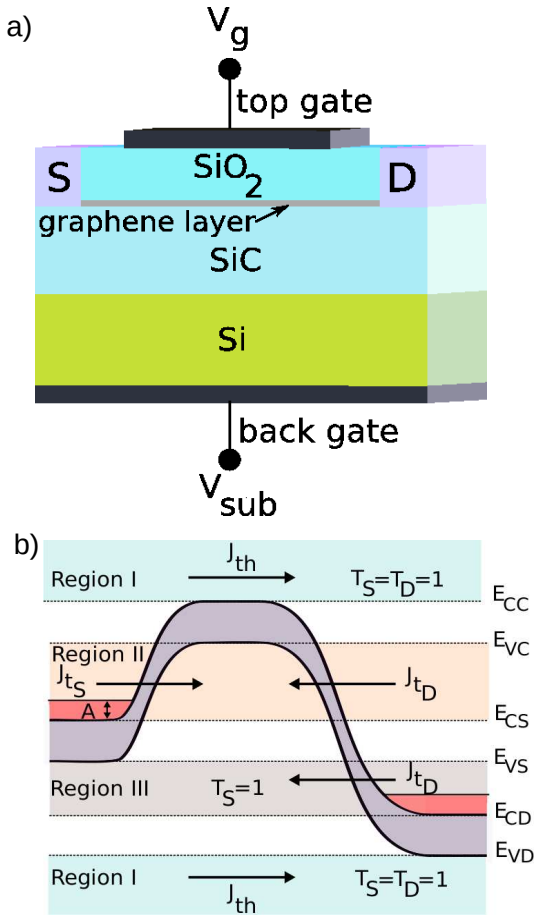

Fig. 1. a) Schematic picture of a graphene on SiC transistor. The grey line between SiO_2 and SiC oxide represents the graphene plane acting as device channel. Source (S) and drain (D) contacts are also in graphene. b) Profile band structure along the transport direction. The dashed lines mark the energy region in which it is possible to have thermionic current (J_{th}), tunneling current from source to channel (J_{tD}) and tunneling current from drain to channel (J_{tS}).

drain, $T_{S,D}$ are the transmission probabilities from source/drain contacts to channel and v_x is the group velocity. $(1-T_S)\, f_-^e v_x$ and $(1-T_D)\, f_+^e v_x$ are the reflected current components from source and drain barriers, respectively. The last term of eqs. 3 and 4 is a thermalization process with the source and drain reservoirs, with characteristic times τ_S and τ_D, respectively. The steady-state f_+^e and f_-^e can be obtained by solving eq. 3 and eq. 4:

$$f_+^e = \frac{\left(T_D + \frac{1}{\tau_D \nu}\right)(1-T_S)\, f_D^e + \left(\frac{1}{\tau_D \nu} + 1\right)\left(T_S + \frac{1}{\tau_S \nu}\right) f_S^e}{\left(\frac{1}{\tau_S \nu} + 1\right)\left(\frac{1}{\tau_D \nu} + 1\right) - (1-T_S)(1-T_D)}, \tag{5}$$

$$f_-^e = \frac{\left(T_S + \frac{1}{\tau_S \nu}\right)(1-T_D)\, f_S^e + \left(\frac{1}{\tau_S \nu} + 1\right)\left(T_D + \frac{1}{\tau_D \nu}\right) f_D^e}{\left(\frac{1}{\tau_S \nu} + 1\right)\left(\frac{1}{\tau_D \nu} + 1\right) - (1-T_S)(1-T_D)}, \tag{6}$$

where $\nu = \frac{2\pi^2 v_x}{L_C}$ is the inverse of the crossing time τ_t. The same reasoning can be applied to derive the hole occupation factors in the channel $f_\pm^h$.

The charge, to be self-consistently solved with eq.2 in order to obtain the channel potential ϕ_{ch}, is computed

through the integration on the BZ

$$\begin{aligned} Q &= -\frac{q}{4\pi^2}\iint_{BZ}\left(f_+^e + f_-^e\right)dk_x dk_y + \\ &+\frac{q}{4\pi^2}\iint_{BZ}\left(f_+^h + f_-^h\right)dk_x dk_y, \end{aligned} \tag{7}$$

where the total current density is expressed as [18]

$$\begin{aligned} J_{tot} &= \frac{q}{4\pi^2}\left\{\iint_{BZ} v_x\left(f_+^e - f_-^e\right)dk_x dk_y \right. \\ &\left. + \iint_{BZ} v_x\left(f_+^h - f_-^h\right)dk_x dk_y\right\} \end{aligned} \tag{8}$$

The transmission probability T_S (T_D) of the interband barrier at source (drain) is zero in the source (drain) band gap and 1 when there is no barrier between source (drain) and channel. When a barrier is present T_S is computed analytically with the WKB approximation, assuming k_y conservation due translational invariance along the y direction:

$$T_S(E,k_y) = \exp\left\{-2\int_{x_1}^{x_2}|Im(k_x^{E,k_y}(x))|dx\right\}, \tag{9}$$

where x_1 and x_2 are the classical turning points, and E is the particle kinetic energy. The same approach is repeated for T_D.

The potential profile between each contact and the central region of the channel is described by an exponential, with characteristic variation length λ, obtained from evanescent mode analysis [19]. Assuming $t_{sub} \gg t_{ox} > t_{ch}$ we obtain:

$$\lambda \approx \left(t_{ox} + \frac{t_{ch}}{2}\right)\frac{2}{\pi}, \tag{10}$$

where t_{ch} is the effective separation between the interfaces of the SiO_2 and SiC layers, for which we assume $t_{ch} = 1$ nm [9].

III. Electrostatics

From analysis of the electrostatics we can gain a better insight of the device performance limitations. In fact gate voltage control upon the channel potential (of which the subthreshold slope S is a measure) is strictly limited by the quantum capacitance C_q of the channel. Device electrostatics can be schematized as in 2(a). The differential

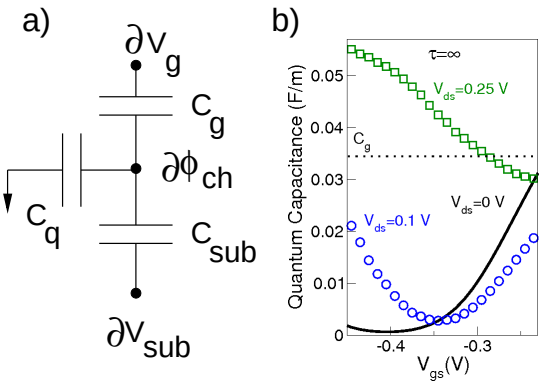

Fig. 2. a) Equivalent circuit of device electrostatics. b) Quantum capacitance-voltage characteristics for $V_{ds} = 0, 0.1, 0.25$ V, $t_{ox} = 1$ nm, $t_{sub} = 100$ nm and $\alpha_D = 9.3 \times 10^{-3}$ in case of fully ballistic transport.

capacitance seen by the gate is

$$C_{tg} = C_g\left(1 - \frac{\partial\phi_{ch}}{\partial V_g}\right) \tag{11}$$

but, from 2(a), C_{tg} can also be expressed in terms of capacitances C_g, C_{sub}, and C_q:

$$C_{tg} = \frac{C_g\,(C_{sub} + C_q)}{C_g + C_{sub} + C_q}. \tag{12}$$

From eqs. (11) and (12) we get the derivative of the channel potential with respect to the gate potential

$$\frac{\partial \phi_{ch}}{\partial V_g} = \frac{C_g}{C_g + C_{sub} + C_q}. \tag{13}$$

The expression of the sub-threshold slope S then turns out to be

$$S = \left(1 + \frac{C_{sub} + C_q}{C_g}\right) \frac{kT}{q} \ln(10), \tag{14}$$

from which it is clear that S is an increasing function of C_q, and therefore a large quantum capacitance severely limits device performance.

2(b) shows the capacitance-gate voltage characteristics for $V_{ds} = 0$, 0.1 and 0.25 V obtained by solving the Schrödinger equation self-consistently with Poisson equation. In the fully ballistic case the quantum capacitance is low for small V_{ds}, indicating a good control of the channel by the gate voltage, but, as soon as V_{ds} increases, hole accumulation in the channel occurs and C_q increases, rapidly degrading S (2(b)). In the inelastic case, instead, the hole accumulation process is slightly suppressed by inelastic injection from the source but the effect on the quantum capacitance is practically negligible. We have observed that for τ larger than 10^{-4} ns, the quantum capacitance basically does not change with respect to 2; on the other hand, for $\tau < 10^{-4}$ ns C_q decreases with respect to the fully ballistic case, but the inelastic process becomes dominant and eq. 14 loses validity.

IV. Perspectives for device operation

In order to evaluate the possible performance of the SiC-graphene FET, we have computed the transfer characteristics by varying three device parameters: drain-source voltage $V_{ds} = (\mu_S - \mu_D)/q$, donor molar fraction at the contacts α_D (and therefore parameter A) and oxide thickness t_{ox}. We also account for different possible values of inelastic time τ. First,in 3, we analyze the trend of the transfer characteristics for different τ for $V_{ds} = 0.25$ V, $t_{ox} = 1$ nm and $\alpha_D = 6.5 \times 10^{-4}$ (corresponding to $A = 0.01$ eV). We observe that for $\tau \geq 1$ ns the transfer

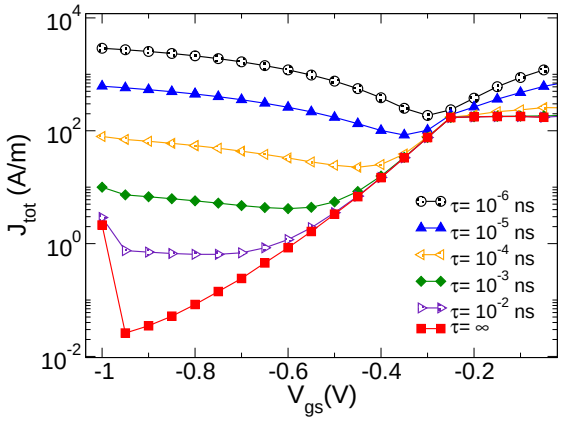

Fig. 3. Transfer-characteristics for $\tau = 10^{-2}, 10^{-3}, 10^{-4}, 10^{-5}, 10^{-6}$ ns, for $V_{ds} = 0.25$ V, $\alpha_D = 6.5 \times 10^{-4}$ and $t_{ox} = 1$ nm.

characteristics are unaffected and identical to the ballistic case ($\tau \to \infty$). Reducing the relaxation time under 1 ns, the minimum current increases and the sub-threshold slope remains almost constant since the quantum capacitance of the channel does not change. The introduction of inelastic scattering process has mainly two effects in the transfer characteristics: one is a gradual change of the current in the sub-threshold region, the other is an increase

of saturation current for $\tau < 10^{-4}$ ns or when inelastic current becomes relevant. In the most favorable case a sub-threshold slope of 140 mV/dec can be obtained.
In 4 we have highlighted the effect of V_{ds} and of the doping level of contacts. As expected the main visible effect of increasing V_{ds} is a gradual degradation of the sub-threshold slope, both in the fully ballistic case (4(a)-(b)) and in the case of relaxation time $\tau = 10$ ps (4(c)-(d)), from 84 mV/dec to 202 mV/dec. The reason is simply related to the increased accumulation of holes in the channel with increasing V_{ds}, which implies a larger quantum capacitance of the channel and therefore a reduced control of the channel potential from the gate voltage.

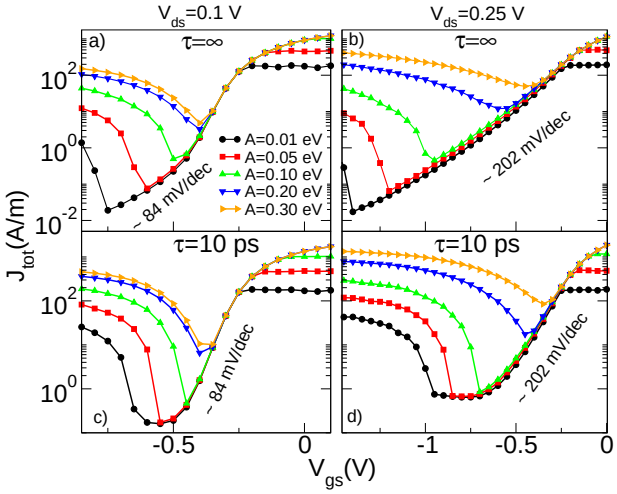

Fig. 4. Transfer characteristics for varying with doping parameter $A = 0.01$, 0.05, 0.1, 0.2, 0.3 eV corresponding respectively to α_D of 6.5×10^{-4}, 4×10^{-3}, 9.3×10^{-3}, 2.3×10^{-2}, 4.3×10^{-2}, $t_{ox} = 2$ nm with: a) $V_{ds} = 0.1$ V, $\tau = \infty$, b) $V_{ds} = 0.25$ V, $\tau = \infty$, c) $V_{ds} = 0.1$ V, $\tau = 10$ ps and d) $V_{ds} = 0.25$ V, $\tau = 10$ ps.

Increasing the doping causes an increase of both the maximum current, due to an improved capacity of the source to inject electrons, and the minimum current. From 4 we draw the indication that by reducing doping at the contacts we improve the current dynamics. As already noted, when the source-drain voltage exceeds the gap of the semiconducting channel ($V_{ds} > 0.26$ V), the characteristics drastically degrade, since band-to-band tunneling current becomes comparable with the thermionic current, and hole accumulation in the channel inhibits channel control from the gate.

The increase of oxide thickness t_{ox} has mainly two effects, which can be associated to a reduction of the capacitive coupling between gate and channel: it increases the sub-threshold slope S (as shown in 5(a)), and the opacity of tunneling barriers (i.e. a larger λ). The former effect is more evident for $V_{ds} = 0.25$ V, where the quantum capacitance is larger, instead S is almost constant at about 75 mV/dec for $V_{ds} = 0.1$ V and $\tau < 10^{-4}$ ns, instead for smaller τ, $S \sim 100$ mV/dec. 5(b) represents the $I_{\rm on}/I_{\rm off}$ ratio as a function of t_{ox} for $V_{ds} = 0.1$ V and $V_{ds} = 0.25$ V, calculated for a gate voltage range $\Delta V_g = 0.25$ V for different values of τ. Larger values of the $I_{\rm on}/I_{\rm off}$ ratio are observed for $\tau = 1$ ns.
From our analysis of transfer characteristics, evaluated by varying three device parameters as V_{ds}, α_D and t_{ox}, we stress the important result that for small V_{ds} and doping level (4(a)) current is modulated by more than 4 orders of magnitude.
We have to stress also the main limitation of graphene on SiC: the energy gap of 0.26 eV coupled to a low effective mass results in a high band-to-band tunneling current $V_{ds} > 0.26$ V and so in an increase of the minimum current achievable. This limitation on V_{ds} affects the perspectives for digital circuit operation: in that case we need $V_{ds} = \Delta V_g$ and equal to the supply voltage. Even for optimized device parameters ($t_{ox} = 1$ nm, $\alpha_D = 4 \times 10^{-3}$), and a supply voltage of 0.25 V, we obtain an $I_{\rm on}/I_{\rm off}$ ratio of 50, as can been seen from 5(b).

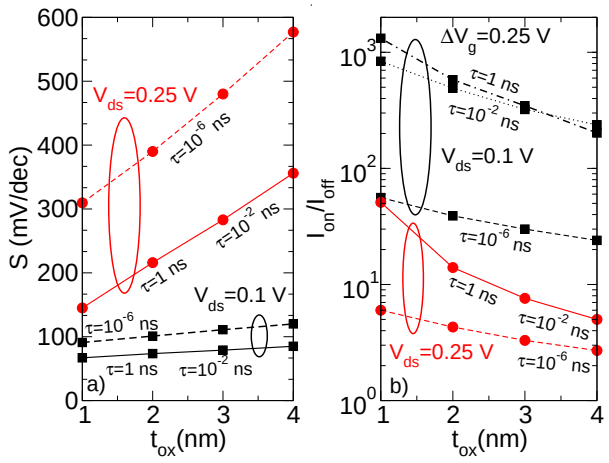

Fig. 5. a) Sub-threshold slope for $V_{ds} = 0.1$ V and $V_{ds} = 0.25$ V calculated with different relaxation time τ. b) $I_{\rm on}/I_{\rm off}$ ratio for $V_{ds} = 0.1$ V and $V_{ds} = 0.25$ V calculated with different relaxation time τ.

V. Conclusion

In this work we have investigated the performance of field-effect transistors based on epitaxial graphene on a SiC substrate with an analytical model. We have shown that, for small V_{ds} and doping level, current is modulated by more than four orders of magnitude: this is a main improvement with respect to other graphene-based devices [20], [21], [16], [15]. Comparable results can be obtained only with carbon nanotubes or graphene nanoribbons, but only with post-selection of devices after fabrication (for proper chirality and/or width). In the case of graphene on SiC, lithography and device patterning are certainly not prohibitive. A steep subthreshold behavior ($S = 67$ mV/decade) can be obtained for small $V_{ds} = 0.1$ V, when the accumulation of holes in the channel is inhibited, and a larger current ratio, in excess of 10^3, can be obtained for a gate voltage window of 0.25 V. For digital applications, the limiting factor is represented by the small voltage drop applicable to the channel, being limited by the energy gap (0.26 eV) of the semiconducting material. With optimized device parameters we have obtained a sub-threshold slope of ≈ 140 mV/decade and an $I_{\rm on}/I_{\rm off}$ equal to 50, with a supply voltage of 0.25 V and $\tau = 1$ ns. This falls short of requirements of the International Technology Roadmap for Semiconductors, which requires $I_{\rm on}/I_{\rm off} \approx 10^4$ [22]. Finally, we believe that graphene on SiC is very promising as a channel material for FETs, and much attention has to be put on mechanisms capable to suppress hole injection also at larger V_{ds}, that would allow to improve the subthreshold swing and obtain a good $I_{\rm on}/I_{\rm off}$ also with a small applied voltage, and on its use in tunnel FETs, where its low gap and low effective mass can be turned into an advantage.

Acknowledgements -The work was supported in part by the the CNR and the EC Sixth Framework Programme, under Contract N. ERAS-CT-2003-980409, through the ESF EUROCORES Programme FoNE-DEWINT, and by the EC Seventh Framework Program under project GRAND (Contract 215752) and the Network of Excellence NANOSIL (Contract 216171).

REFERENCES

[1] S. Y. Zhou, G. H. Gweon, A. V. Fedorov, P. N. First, W. A. de Heer, D. H. Lee, F. Guinea, A. Castro Neto, and A. Lanzara, "Substrate-induced bandgap opening in epitaxial graphene," *Nat. Mat.*, vol. 6, no. 10, p. 770, Oct. 2007.

[2] X. Peng and R. Ahuja, "Symmetry breaking induced bandgap in epitaxial graphene layers on SiC," *Nano Lett.*, vol. 8, no. 12, p. 4464, Oct. 2008.

[3] S. Kim, J. Ihm, H. J. Choi, and Y.-W. Son, "Origin of anomalous electronic structures of epitaxial graphene on Silicon Carbide," *Phys. Rev. Lett.*, vol. 100, no. 17, p. 176802, 2008.

[4] V. W. Brar, Y. Zhang, Y. Yayon, T. Ohta, J. L. McChesney, A. Bostwick, E. Rotenberg, K. Horn, and M. F. Crommie, "Scanning tunneling spectroscopy of inhomogeneous electronic structure in monolayer and bilayer graphene on sic," *App. Phys. Lett.*, vol. 91, no. 12, p. 122102, 2007. [Online]. Available: http://link.aip.org/link/?APL/91/122102/1

[5] P. Kedzierski, J.and Pei-Lan Hsu; Healey, P. Wyatt, C. Keast, M. Sprinkle, C. Berger, and W. de Heer, "Epitaxial graphene transistors on sic substrates," *IEEE TED*, vol. 55, no. 8, p. 2078, 2008.

[6] K. S. Novoselov, A. K. Geim, S. V. Morozov, D. Jiang, Y. Zhang, S. V. Dubonos, I. V. Grigorieva, and A. A. Firsov, "Electric field effect in atomically thin carbon films," *Science*, vol. 306, no. 5696, p. 666, Oct. 2004.

[7] K. S. Novoselov, A. K. Geim, S. V. Morozov, D. Jiang, M. I. Katsnelson, I. V. Grigorieva, S. V. Dubonos, and A. A. Firsov, "Two-dimensional gas of massless Dirac fermions in graphene," *Nature*, vol. 438, no. 7065, p. 197, 2005.

[8] A. K. Geim and K. S. Novoselov, "The rise of graphene," *Nat. Mat.*, vol. 6, no. 3, p. 183, Mar. 2007.

[9] X. Li, X. Wang, L. Zhang, S. Lee, and H. Dai, "Chemically Derived, Ultrasmooth Graphene Nanoribbon Semiconductors," *Science*, vol. 319, no. 1229, p. 1150878, 2008.

[10] F. Schedin, A. K. Geim, S. V. Morozov, E. W. Hill, P. Blake, M. I. Katsnelson, and K. S. Novoselov, "Detection of individual gas molecules adsorbed on graphene," *Nat Mater*, vol. 6, no. 9, p. 652, 2007.

[11] Y.-W. Son, M. L. Cohen, and S. G. Louie, "Energy gaps in graphene nanoribbons," *Phys. Rev. Lett.*, vol. 97, no. 21, p. 216803, 2006.

[12] R. Martel, T. Schmidt, H. R. Shea, T. Hertel, and P. Avouris, "Single- and multi-wall carbon nanotube field-effect transistors," *App. Phys. Lett.*, vol. 73, no. 17, p. 2447, 1998. [Online]. Available: http://link.aip.org/link/?APL/73/2447/1

[13] B. Biel, X. Blase, F. Triozon, and S. Roche, "Anomalous doping effects on charge transport in graphene nanoribbons," *Phys. Rev. Lett.*, vol. 102, no. 9, p. 096803, 2009. [Online]. Available: http://link.aps.org/abstract/PRL/v102/e096803

[14] T. Ohta, A. Bostwick, T. Seyller, K. Horn, and E. Rotenberg, "Controlling the electronic structure of bilayer graphene," *Science*, vol. 313, no. 5789, pp. 951–954, August 2006.

[15] G. Fiori and G. Iannaccone, "On the possibility of tunable-gap bilayer graphene FET," *IEEE EDL*, vol. 30, no. 3, p. 261, Mar. 2009.

[16] Y. Q. Wu, P. D. Ye, M. A. Capano, Y. Xuan, Y. Sui, M. Qi, J. A. Cooper, T. Shen, D. Pandey, G. Prakash, and R. Reifenberger, "Top-gated graphene field-effect-transistors formed by decomposition of sic," *App. Phys. Lett.*, vol. 92, no. 9, p. 092102, 2008.

[17] G. Fiori and G. Iannaccone, "Simulation of graphene nanoribbon field-effect transistors," *IEEE EDL*, vol. 28, no. 8, p. 760, 2007.

[18] M. Buttiker, "Coherent and sequential tunneling in series barriers," *IBM J.Res.Dev.*, vol. 32, no. 1, p. 63, 1988.

[19] S.-H. Oh, D. Monroe, and J. Hergenrother, "Analytic description of short-channel effects in fully-depleted double-gate and cylindrical, surrounding-gate mosfets," *IEEE EDL*, vol. 21, no. 9, p. 445, Sep. 2000.

[20] M. Lemme, T. Echtermeyer, M. Baus, and H. Kurz, "A graphene field-effect device," *IEEE EDL*, vol. 28, no. 4, p. 282, April 2007.

[21] X. Liang, Z. Fu, and S. Y. Chou, "Graphene transistors fabricated via transfer-printing in device active-areas on large wafer," *Nano Lett.*, vol. 7, no. 12, p. 3840, December 2007. [Online]. Available: http://dx.doi.org/10.1021/nl072566s

[22] "International technology roadmap for semiconductor 2007." [Online]. Available: http://public.itrs.net.